UC Berkeley

UC Berkeley Previously Published Works

Title

Field-scale soil carbon analysis: Correcting for moisture and bulk density effects in Inelastic Neutron Scattering

Permalink

https://escholarship.org/uc/item/2hc9f66v

Journal

Soil and Tillage Research, 266

ISSN

0167-1987

Authors

Larsen, William

Smykalov, Valerie

Castanha, Cristina

et al.

Publication Date

2027-02-01

DOI

10.1016/j.still.2026.107459

Copyright Information

This work is made available under the terms of a Creative Commons Attribution License, available at https://creativecommons.org/licenses/by/4.0/

Peer reviewed

eScholarship.org Powered by the California Digital Library
University of California

Soil & Tillage Research 266 (2027) 107459

Contents lists available at ScienceDirect

Soil & Tillage Research

journal homepage: www.elsevier.com/locate/still

Field-scale soil carbon analysis: Correcting for moisture and bulk density effects in Inelastic Neutron Scattering

William Larsen [a,1], Valerie Smykalov [a,2], Cristina Castanha [b], Eoin Brodie [b], Mauricio Ayllon Unzueta [a], Bernhard Ludewigt [a], Arun Persaud [a,*]

[a] Accelerator Technology and Applied Physics Division, Lawrence Berkeley National Laboratory, 1 Cyclotron Road, Berkeley, 94720, CA, USA
[b] Earth and Environmental Sciences, Lawrence Berkeley National Laboratory, 1 Cyclotron Road, Berkeley, 94720, CA, USA

ARTICLE INFO

Keywords:
Inelastic neutron scattering
Associated particle imaging
Soil carbon
Neutron attenuation
Monte Carlo simulation
MCNP

ABSTRACT

Traditional point-sampling methods for soil elemental analysis often struggle to capture field-scale spatial variations and rely on destructive, labor-intensive bulk density measurements. Inelastic Neutron Scattering (INS) offers rapid, non-destructive, *in situ* measurements of soil elemental composition over large volumes. A unique advantage of this neutron-based method is the potential to measure all major soil components simultaneously, allowing for the simultaneous estimation of bulk density and water content alongside elemental carbon. While standard INS yields bulk concentrations over a given volume, spatially resolved measurements require techniques such as Associated Particle Imaging (API). INS-API techniques provide non-destructive access to depth-resolved information, but the quantitative accuracy of this technique depends heavily on correcting for signal attenuation. While gamma-ray attenuation is readily predicted from soil density, neutron attenuation is complex and highly sensitive to hydrogen content, confounding carbon measurements in soils. In this study, we use Monte Carlo simulations of soils with varied compositions, bulk densities, and water contents to model neutron attenuation and develop a simple predictive model requiring only dry bulk density and volumetric water content. We find that such a simplification achieves accuracy within 10% at 30 cm depth for simulated soils, and validate the model experimentally to 18 cm depth using an INS–API system with controlled soil columns. This approach enables practical correction of INS–API measurements, laying the groundwork for a self-consistent framework to monitor soil carbon stocks independent of moisture fluctuations.

1. Introduction

Soil carbon (C) is a key component of soil health (Lal, 2014) and one of the largest terrestrial reservoirs of C, exchanging rapidly with atmospheric CO_2 (Padarian et al., 2022). However, accurately determining soil C stocks remains a logistical challenge (Paustian et al., 2019). Current methods for determining soil C rely on point sampling of soil cores and laboratory analysis, which are time-consuming, expensive, and spatially limited. Crucially, converting C concentration (%) to stocks requires accurate bulk density measurements, which are laborious to collect and often introduce significant uncertainty into the measurements.

Inelastic Neutron Scattering (INS) analysis offers a non-destructive, field-based alternative for measuring elemental composition in soils (Wielopolski et al., 2011; Ayllon Unzueta et al., 2019, 2021; Kavetskiy et al., 2026). High-energy (14.1 MeV) neutrons are directed toward the soil, where they collide with nuclei, producing characteristic prompt gamma rays—such as the 4.43 MeV signature for carbon (Wielopolski et al., 2000). Unlike coring, INS integrates over large soil volumes (~0.3 m^3) (Wielopolski et al., 2008), typically sensing to ~30 cm depth (Wielopolski and Doron, 2012; Yakubova et al., 2022, 2025), but the bulk measurement is dominated by the upper 0 cm to 10 cm (Yakubova et al., 2016). This depth dependence reflects attenuation of both high-energy neutrons and the emitted gamma rays.

Associated Particle Imaging (API) enhances INS by detecting the alpha particle emitted in coincidence with each neutron from the D–T fusion reaction (Ayllon Unzueta et al., 2021). The alpha particle provides the neutron's initial trajectory and, combined with the gamma ray detection time, allows for reconstruction of the scattering location in three dimensions with centimeter resolution. This enables accurate voxelated 3D imaging of elemental distributions to ~30 cm depth. In

* Corresponding author.
E-mail address: apersaud@lbl.gov (A. Persaud).
[1] Now at: Terradot, San Francisco, CA, USA.
[2] Now at: Department of Civil and Environmental Engineering, Penn State University, University Park, PA, USA.

https://doi.org/10.1016/j.still.2026.107459
Received 4 March 2026; Received in revised form 14 August 2026; Accepted 30 August 2026
Available online 15 September 2026
0167-1987/Published by Elsevier B.V. This is an open access article under the CC BY license (http://creativecommons.org/licenses/by/4.0/).

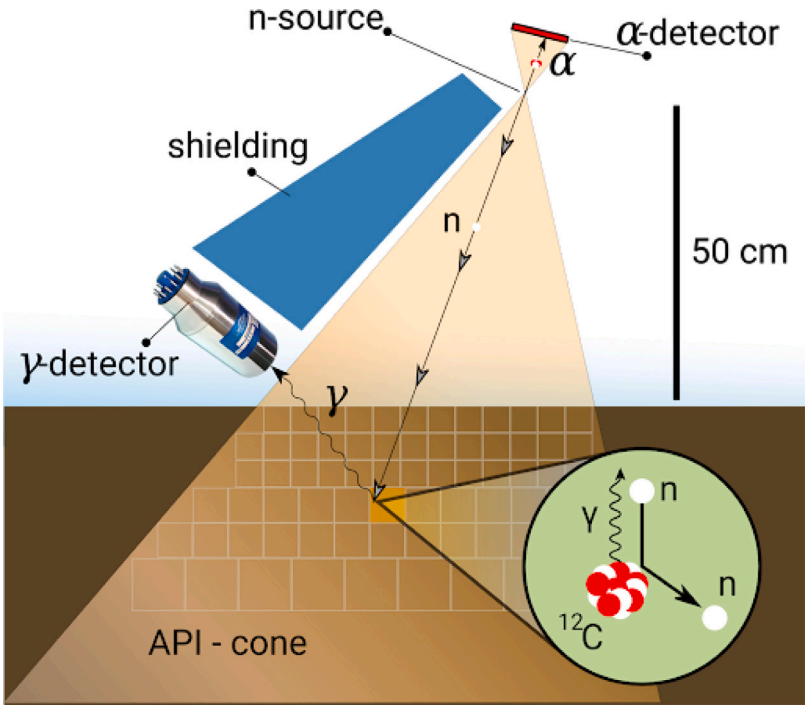


Fig. 1. Schematic of the INS–API system showing the emission of a 14.1 MeV neutron and associated 3.5 MeV alpha particle from the D–T reaction. The alpha particle is detected by a YAP scintillator, providing the neutron's initial trajectory and time of emission, while gamma rays from neutron interactions in the soil are detected by $LaBr_3$ and NaI scintillators.

contrast to combustion or spectroscopic techniques that rely on point sampling of small volumes (Sorenson et al., 2018; Paustian et al., 2019), INS-API allows for completely non-destructive sampling of large samples (~400 kg of soil). A schematic of an API-INS system is shown in Fig. 1 displaying the main components of the system and the voxelated soil volume. The position of the alpha detector and the small point-like source of D-T fusion reactions define a volume, called the API-cone, in the soil/target area to which the system is sensitive.

Recent advances in soil carbon mapping algorithms can achieve a much finer spatial resolution over large regions (de Gruijter et al., 2018), but their accuracy depends on dense, high-quality ground-truth measurements (Viscarra Rossel et al., 2016; Stanley et al., 2023). Current core sampling and laboratory analysis workflows do not scale well to the large number of measurements needed within smaller areas, limiting the reliability of such models while also requiring extra measurements such as bulk density (Paustian et al., 2019). Fast, non-destructive methods such as INS–API are therefore critical for providing the spatially rich datasets these models require.

A unique and powerful advantage of neutron-based methods is the capability to measure all major soil constituents (Si, O, Al, Fe, etc.) simultaneously. This offers a pathway toward a *self-consistent* measurement framework: by summing the masses of the detected elements, the system can estimate soil bulk density directly from the spectra, eliminating the need for separate physical density measurements.

The quantitative accuracy of INS–API measurements at depth is heavily influenced by signal attenuation. While gamma-ray attenuation is a straightforward function of total density, neutron attenuation is complex and dominated by hydrogen content (Wielopolski et al., 2005). In agricultural soils, hydrogen pools vary dynamically due to precipitation (pore water), mineralogy (lattice water), and organic matter content. If not corrected, high moisture content can significantly dampen the neutron flux at depth, leading to an underestimation of carbon stocks in deeper soil layers. This is particularly problematic for monitoring campaigns that must operate in different seasons or moisture regimes.

Recent work by Yakubova et al. (2025) demonstrated that neutron-gamma signals can be used to map soil moisture. Building on this, accurate carbon quantification requires a robust model to inversely correct for that moisture-driven attenuation. Kavetskiy et al. (2026) recently applied a correction equation developed in Kavetskiy et al. (2024) which accounts for bulk density and soil moisture to 16 soils in field conditions. Expanding on this, here we utilize Monte Carlo N-Particle (MCNP) simulations (Goorley et al., 2012) to model neutron attenuation with depth across 33 distinct soil types with varied bulk densities and water contents. We explicitly account for hydrogen contributions from free water, lattice water, and organic matter. To determine whether a simple neutron attenuation correction is suitable for diverse soil types, we use MCNP to develop a simplified empirical model that predicts neutron attenuation to a depth of 30 cm using only dry bulk density and volumetric water content. We validate this model experimentally using an INS–API system (Ayllon Unzueta et al., 2019, 2021) in controlled soil columns to a depth of 18 cm. We discuss how this validated correction framework acts as a prerequisite for self-consistent, non-destructive monitoring of soil carbon stocks and other elements under variable field conditions.

2. Materials and methods

2.1. Gamma-ray attenuation coefficients

The attenuation of gamma rays through soil is described by the mass attenuation coefficient (μ_m, $cm^2\ g^{-1}$), which quantifies the probability of gamma interaction per unit mass. We retrieved μ_m values for individual elements from the NIST XCOM database (Berger et al., 2010) and interpolated between the tabulated 4 MeV and 5 MeV values to calculate μ_m for 4.4 MeV. For each soil, a composite μ_m was calculated from the elemental abundances (wt.%) listed in Table 1. The linear attenuation coefficient (μ, cm^{-1}) was then calculated as:

$$\mu = \mu_m \cdot \rho_{\text{total}}, \tag{1}$$

Table 1
Bulk properties and mass fractions of selected isotopes used for MCNP simulations of soils. Four synthetic soils span a broad range of bulk density and water content, while lattice water and organic carbon are set to the mean of observations from Franz et al. 2013. The mean and range (minimum to maximum) for the observations from Franz et al. 2013 are shown in the rightmost column. Note that bulk properties are shown with standard units to maintain practical interpretability.

		Synthetic soils				Franz et al. (2013) soils (n=33)
Bulk properties	Units	Dry porous	Dry dense	Wet porous	Wet dense	Average (min–max)
Dry bulk density	g soil cm^{-3} total	1.1	1.5	1.1	1.5	1.313 (0.885–1.577)
Volumetric water content	cm^3 H_2O cm^{-3} total	0	0	0.4	0.4	0.235 (0.051–0.481)
Lattice water content	g H_2O g^{-1} soil	0.037	0.037	0.037	0.037	0.037 (0.003–0.064)
Organic carbon content	g C g^{-1} soil	0.016	0.016	0.016	0.016	0.016 (0.002–0.081)
Mass fractions						
^{16}O	g g^{-1} total	0.521	0.521	0.616	0.596	0.574 (0.523–0.634)
^{28}Si	g g^{-1} total	0.327	0.327	0.242	0.260	0.282 (0.173–0.426)
^{27}Al	g g^{-1} total	0.058	0.058	0.043	0.046	0.049 (0.001–0.091)
^{56}Fe	g g^{-1} total	0.032	0.032	0.023	0.025	0.027 (0.004–0.072)
^{39}K	g g^{-1} total	0.007	0.007	0.005	0.006	0.006 (0–0.021)
^{23}Na	g g^{-1} total	0.009	0.009	0.006	0.007	0.007 (0–0.021)
^{40}Ca	g g^{-1} total	0.012	0.012	0.009	0.009	0.010 (0–0.074)
^{24}Mg	g g^{-1} total	0.006	0.006	0.004	0.005	0.005 (0–0.014)
^{48}Ti	g g^{-1} total	0.004	0.004	0.003	0.003	0.003 (0.001–0.008)
^{12}C	g g^{-1} total	0.019	0.019	0.014	0.015	0.015 (0.002–0.058)
^{1}H	g g^{-1} total	0.006	0.006	0.033	0.027	0.021 (0.006–0.042)

where ρ_{total} is the total density of solids and liquids in the soil (dry solids + water).

Applying a generic mass attenuation rate (μ_m) to a soil of unknown composition requires the assumption that gamma attenuation at these energies is dominated by Compton scattering and pair production, both of which scale with electron density, and thus with total material density rather than specific composition (Akar Tarim et al., 2013). As we show later, μ_m varies little between soils, reinforcing the use of ρ_{total} as the primary control on gamma attenuation.

2.2. Soil dataset and synthetic soils

We used a dataset (Franz et al., 2013) that provides a complete set of soil properties for 33 U.S. soils, including dry bulk density (ρ_{bd}, in g per cm^3 of soil), volumetric water content (VWC, θ, in cm^3 of water per cm^3 of soil), lattice water content (LWC, in g water per g of soil), and organic carbon (in g C per g of soil). These soils span a wide range of textures, mineralogies, and organic matter contents. This dataset is valuable because accurate neutron transport modeling requires a full accounting of hydrogen sources. While bulk density and VWC are often measured, LWC and organic matter content are rarely reported together, despite both contributing hydrogen atoms that strongly affect neutron moderation (Wielopolski et al., 2005).

In addition to these natural soils, we evaluated four "synthetic soils" to isolate the effects of ρ_{bd} and θ. Modeled synthetic soils had constant LWC and organic matter (set to the mean of the dataset) but varied ρ_{bd} and θ in increments of $0.4\,g\,cm^{-3}$ and $0.4\,cm^3\,cm^{-3}$, respectively. This allowed for direct comparison of the attenuation effects of solid vs. water mass increases at equal density increments. In Table 1 we present a summary of the soil properties of the modeled soils, as well as the elemental abundances of the soil mixture used as the MCNP input.

2.3. Accounting for hydrogen sources

Hydrogen content in soils was calculated from three components:

1. Free water: reported as VWC (θ, volume of water per volume of soil), converted to water mass per volume of soil using water density. This factor may change rapidly with time, depending on rainfall amounts and soil water retention characteristics, but evaluated soils primarily lie within the range of 0 to 50%.
2. Lattice water: hydroxyl groups bound in mineral lattices, expressed as LWC (g H_2O per g soil material).
3. Organic matter hydrogen: estimated from organic carbon content (reported as g C per g soil material), assuming cellulose composition ($C_6H_{10}O_5$) (Wielopolski et al., 2005), which has a high H:C ratio and thus represents a maximum plausible hydrogen content from organic matter. The resulting organic matter water content can be reported in g H_2O per g soil material.

Conversion of the three water sources listed in Table 1 to common mass ratio units (g H_2O per g soil material) yields free water contents of 0–0.48, lattice water contents of 0–0.06, and organic water contents from 0–0.10. For the evaluated soils, free water constitutes an average of 70% of the total water content when considered in this way. This explicit accounting is important because hydrogen's large scattering cross section makes it the dominant moderator of fast neutrons. Even small errors in hydrogen estimation can lead to significant neutron attenuation prediction errors.

2.4. MCNP simulation setup

We used MCNP 6.1 (Goorley et al., 2012) with ENDF/B-VIII.0 nuclear data libraries (Brown et al., 2018) to simulate neutron and gamma transport. The geometry was a homogeneous $200\,cm \times 200\,cm \times 100\,cm$ soil block, with an isotropic 14.1 MeV neutron source located 60 cm above the surface. Each soil simulation used 2×10^9 neutrons. We did not model detector housings or shielding, focusing solely on particle transport in soil. The chemical composition of a simulated material was designated by mass fractions of individual isotopes in the MCNP input file, and the total density was specified separately. Soil is a mixture of different components: we added together the chemical compositions of the solid material, water content, and organic matter into a scaled weight percent array for each element. We simulated only 11 elements and only the major stable isotope for each (e.g., ^{16}O) because trace elements (e.g., Cd or Zn) or rare stable isotopes (e.g., ^{18}O) are typically less abundant by orders of magnitude in natural soils.

Gamma ray production from $^{12}C(n,n'\gamma)$ reactions was tallied using an F4 mesh tally with FM multipliers for the reaction cross section, in 1 cm vertical bins down to 60 cm depth. From the results, we calculated the INS reaction rate given in gammas/cm^3/(source neutron). The FM tag enables transformation of the neutron flux from the F4 tally into the reaction rate (RR) of INS reaction (Doron, 2007):

$$RR_i = N_i \int_0^\infty \sigma_i(E)\,\phi(E)\,dE, \tag{2}$$

where ϕ is the neutron flux and σ_i is the energy-dependent cross-section for a neutron collision with some element i. N_i is the number density of the subject atom, calculated as

$$N_i = \frac{w_i \, \rho_{total} \, N_A}{M_i}, \tag{3}$$

where w_i is the weight fraction of the element i in the modeled soil material, ρ_{total} is the total density (g cm^{-3}), M_i is the molar mass of element i (g mol^{-1}), and N_A is Avogadro's constant (6.022×10^{23} mol^{-1}), yielding N_i in units of atoms cm^{-3}. Applying a unit conversion (1 barn = 1×10^{-24} cm^2) allows for the expression of N_i in practical units of atoms barn^{-1} cm^{-1}.

We calculated the reaction rate for INS reactions with C that produce 4.43 MeV gamma rays in the superimposed mesh tally structure grouped into 1 cm^3 voxel cells. The output file `meshtal` reports the reaction rate for cells of different positions X, Y, Z as well as energy bins that correspond to the energy of the incident neutron. To observe the attenuation of the INS reaction rate through the soil column, we summed reaction rates in each voxel across X and Y to yield the change in reaction rate with depth Z. For comparison of soils with different amounts of the INS subject element (i.e., carbon-rich or carbon-poor soils), we normalized reaction rates calculated at depth to that of the surface at 0 cm. This allowed for comparison of fractional attenuation of INS reaction rates with depth.

Application of the INS-API method involves the assumption that the initial neutron travel direction (as inferred from the alpha detector) is not modified prior to generating a gamma ray via the INS reaction. In other words, all detected gamma rays are generated via scattering reactions by neutrons that have not had any collisions that dramatically alter the direction of travel. It is likely that 14.1 MeV neutrons may undergo one or more collisions that lower the neutron energy by a small enough extent that it may later generate a gamma ray (i.e., if it stays above the minimum energy for incident neutrons to undergo an INS reaction, 4.81 MeV for the case of carbon). For a rough approximation of the rate of INS reactions induced by nominally "uncollided" neutrons, a narrow energy bin of 14.0 MeV to 14.1 MeV was set. Since the average decrement of energy per collision of 14.1 MeV neutrons in soil is much higher than 0.1 MeV (Spielberg and Duneer, 1958), this bin likely encompassed all neutrons that have not collided and reduced in energy from 14.1 MeV. We summed reaction rates for all incident energies to represent the total reaction rate. We then compared "uncollided" (14.0 MeV to 14.1 MeV) with the total reaction rate vs. depth to determine the approximate contribution of each group to the INS reaction rate trends observed.

2.5. Fitting attenuation curves

To generate a first-order prediction of the attenuation of 4.43 MeV gamma reaction rates with depth in soil, we fit a function to describe the normalized reaction rate (relative to the surface) at different depths for each modeled soil. The exponential function is useful for describing the attenuation of a mono-energetic particle (e.g., attenuation of gamma rays):

$$RR_{norm}(z) = a \cdot \exp\left(\frac{-z}{b}\right), \tag{4}$$

However, the INS reaction for C that generates 4.43 MeV gamma rays can be initiated by neutrons of varying energies. While the cross-section for ^{12}C(n,n'γ) is continuous from incident neutron energies 4.81 to greater than 14.1 MeV, we found that a double-exponential function describing two modes of attenuation (e.g., primary uncollided 14.1 MeV and secondary collided neutrons) is sufficient to represent the attenuation of the C INS reaction rate:

$$RR_{norm}(z) = a \cdot \exp\left(\frac{-z}{b}\right) + (1-a) \cdot \exp\left(\frac{-z}{c}\right), \tag{5}$$

where a is analogous to a buildup factor, and b and c are attenuation lengths for the two modes of attenuation.

First, we fit Eq. (5) to the reaction rate data vs. depth to obtain attenuation parameters (a, b, and c) for all modeled soils. We then regressed a, b, and c against the bulk density (ρ_{bd}) and water content (θ):

$$i = d_i \, \rho_{bd} + e_i \, \theta + f_i, \tag{6}$$

where $i \in \{a, b, c\}$ and d_i, e_i, and f_i are fitted constants.

After generating predictive estimates of neutron attenuation by fitting to bulk density (ρ_{bd}) and soil water content (θ), we explored whether other sources of water (e.g., lattice water or organic water) are sufficiently abundant to require additional consideration. For this, we also tested effective ρ^*_{bd} and θ^* values including lattice and organic water in Eq. (6):

$$\rho^*_{bd} = \rho_{bd} \cdot (1 - LW - M_{OM} \cdot OW), \tag{7}$$

$$\theta^* = \theta + \rho_{bd} \cdot LW + \rho_{bd} \cdot M_{OM} \cdot OW, \tag{8}$$

where LW is lattice water fraction, M_{OM} is organic matter mass fraction, and OW is organic water fraction (from cellulose stoichiometry).

2.6. Experimental validation

We validated the model using the INS–API system described in Ayllon Unzueta et al. (2019, 2021), with a DT108API neutron generator (Adelphi Technologies Inc.), $LaBr_3$ (3" Saint-Gobain, B390S) and NaI (5" Alpha Spectra, Inc. 20I20/5(9823)BN) gamma detectors, and a YAP scintillator (Crytor Inc.) and a position-sensitive photo multiplier tube (Hamamatsu H13700-03).

Two experiments were conducted to validate the neutron attenuation model: First, the effects of moisture variation were evaluated by adjusting volumetric water content (θ) to 2.6, 11.1, 22.8, 33.1% with a fixed soil depth of 10 cm. Second, attenuation with depth was evaluated for dry soil (θ = 2.6%) over a soil depth range of 3 cm to 18 cm.

The experimental setup is shown in Fig. 2. To avoid complications from additional gamma attenuation and to focus on signals of C in soil (our main interest), we placed a container with soil of varying thickness and moisture level above a carbon block (made of graphite) and isolated API signals from the carbon block only. The soil container attenuated the neutron flux hitting the carbon block, but since we did not have any soil between the carbon block and the gamma detectors, the gamma signal was not attenuated. We chose a water-tight, 40 cm × 40 cm × 20 cm box made from 1.25 mm thick steel to hold the soil. We used a steel container, rather than plastic, to minimize C-bearing material in the experimental setup. The background signal from the empty container was subtracted from each run to minimize the influence of the container itself. Such a background correction is practical, but not perfect, since we acknowledge that the neutron flux on the container will vary with the soil used and between a measurement with soil and without soil.

The soil used was sandy loam (65.8% sand, 18.0% silt, 16.2% clay). Prior to its use in these experiments, the soil was sifted to <2 mm for large pebbles and roots, making it largely uniform in composition and geometry. The bulk density of soil, measured as the weight of dry soil mass divided by volume for each experimental container, ranged from 1.03 to 1.20 g cm^{-3} (average 1.11 g cm^{-3}). The initial moisture content of the soil was measured by weighing six 8 g samples of soil drawn from the sifted source soil, oven drying the samples at 105 °C for 16 h, then weighing them again. We used the average of these values for the initial moisture content of the bulk soil container (2.6 % volumetric water content).

We filled the steel container to 10 cm depth with sifted soil and added water using a water misting apparatus which gradually and uniformly moistened the soil. We used a scale to measure the total amount of water added. We tested incremental volumetric water contents of 11.1%, 22.8%, and 33.1%. At each increment, we sealed the

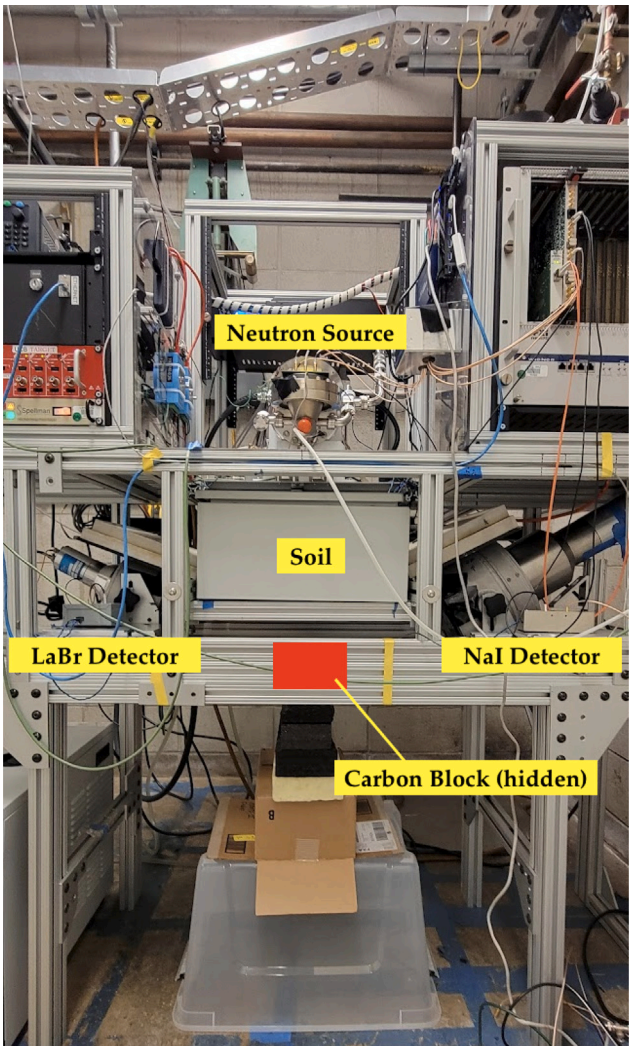


Fig. 2. Experimental setup for neutron attenuation measurements. A steel soil container is placed between the neutron source and a carbon block (graphite) target. Soil depth and moisture were varied to assess their effect on neutron attenuation.

container and waited one hour for the water to percolate uniformly into the soil. As soon as the moisture content became uniform, we placed and centered the soil container under the neutron source with a distance of 27 cm between the neutron production target and the top of the container. To isolate the effect of attenuating material depth on neutron attenuation, we took additional measurements at varying depths of sifted dry (2.6% VWC) soil. We tested depths of 3 cm, 5 cm, 15 cm, and 18 cm and used the same spatial set-up as for the moist soil measurements.

For each measurement, we took one two-hour measurement of just the box containing the soil, and one two-hour measurement of a 20 cm× 13 cm × 6 cm carbon (graphite) block placed on low-density foam so that it was centered 13 cm under the bottom of the soil container (Fig. 2). The first two-hour run provided background scattering from the attenuating material itself that we later subtracted from the measured 4.43 MeV gamma peak.

After the measurements were completed, we estimated the neutron flux going into the carbon block by integrating the 4.43 MeV carbon gamma energy peak, including the first escape peak and the Compton edge, over the volume of the block (Fig. 3). The voxel shape was determined by maximizing the area in XZ and YZ that did not cross over the edge of the API cone. We extended the volume of the voxel in the negative Z direction to capture scattering from the carbon block. We normalized this value to the number of alpha particles detected in the run, with alpha particles taken as a 1:1 proxy for generated neutrons. We did the same for the background measurement and subtracted it from the run with the carbon block to remove background scattering from measurements of carbon counts. This produced a value of normalized neutron flux for each moisture increment. Neutron attenuation was calculated as the normalized neutron flux for each moisture content divided by the normalized neutron flux for the empty steel box measurement.

3. Results

3.1. Simulation results

The attenuation of high-energy (>∼1 MeV) gamma rays through soil shows minimal dependence on soil composition. For all soils tested, the mass attenuation coefficient μ_m for 4.43 MeV gamma rays varied little (Fig. 4a). This reflects the fact that at these energies, Compton scattering dominates, and cross sections are relatively insensitive to atomic number for the light and medium elements common in soil (Akar Tarim et al., 2013). Because the linear attenuation coefficient μ is simply μ_m multiplied by the total density of material, μ is strongly correlated with ρ_{total} (Fig. 4b). This confirms that gamma attenuation can be reliably estimated from density measurements alone, without detailed knowledge of composition, a technique that is also used, for example, in oil exploration (Alger and Raymer, 1963; Borsaru et al., 1985).

The measured rate of INS reactions from C as a function of depth is more complex than pure gamma attenuation due to the soil between the origin of the gamma and the detector because 4.43 MeV gammas can be generated by neutrons over a range of incident energies (4.81 MeV to >14.1 MeV). Neutrons may undergo several collisions and lose energy before producing a gamma ray. Fig. 5a shows normalized reaction rates for four synthetic soils designed to isolate the effects of bulk density and water content. Increasing ρ_{bd} by 0.4 g cm^{-3} (porous → dense) reduced the reaction rate moderately, but increasing θ by the same mass-equivalent density (0.4 g cm^{-3}) had a much stronger effect, illustrating hydrogen's efficiency as a neutron moderator.

For uncollided 14.1 MeV neutrons (Fig. 5b), attenuation follows a near-exponential decay, as expected for monoenergetic particles. The steeper slope in wetter soils reflects the rapid moderation of fast neutrons by hydrogen in water. The fraction of 4.43 MeV gamma rays produced by uncollided neutrons decreases with depth (Fig. 6). In wet soils, this drop is rapid, indicating that most gammas at depth are generated by neutrons that have already scattered and lost energy.

3.2. Regression model performance

We fitted the double-exponential model using Eq. (5) to simulated attenuation curves for 33 real soils (Franz et al., 2013). Regression of a, b, and c against ρ_{bd} and θ using Eq. (6) predicted attenuation curves with percent errors generally < ±10% at 30 cm depth (Fig. 7a) and smaller errors at shallower depth. The result of the regression model is summarized in Table 2. Fitted values for a ranged from −0.31 to −0.06, b ranged from 2.16 cm to 4.07 cm, and c ranged from 11.71 cm to 20.90 cm. Including lattice and organic water in effective ρ^*_{bd} and θ^* improved predictions slightly (Fig. 7b), especially for clay-rich or organic-rich soils. Larger errors occurred in soils with extreme combinations of low ρ_{bd} and high θ, suggesting secondary influences from other elements (e.g., Fe) on neutron attenuation.

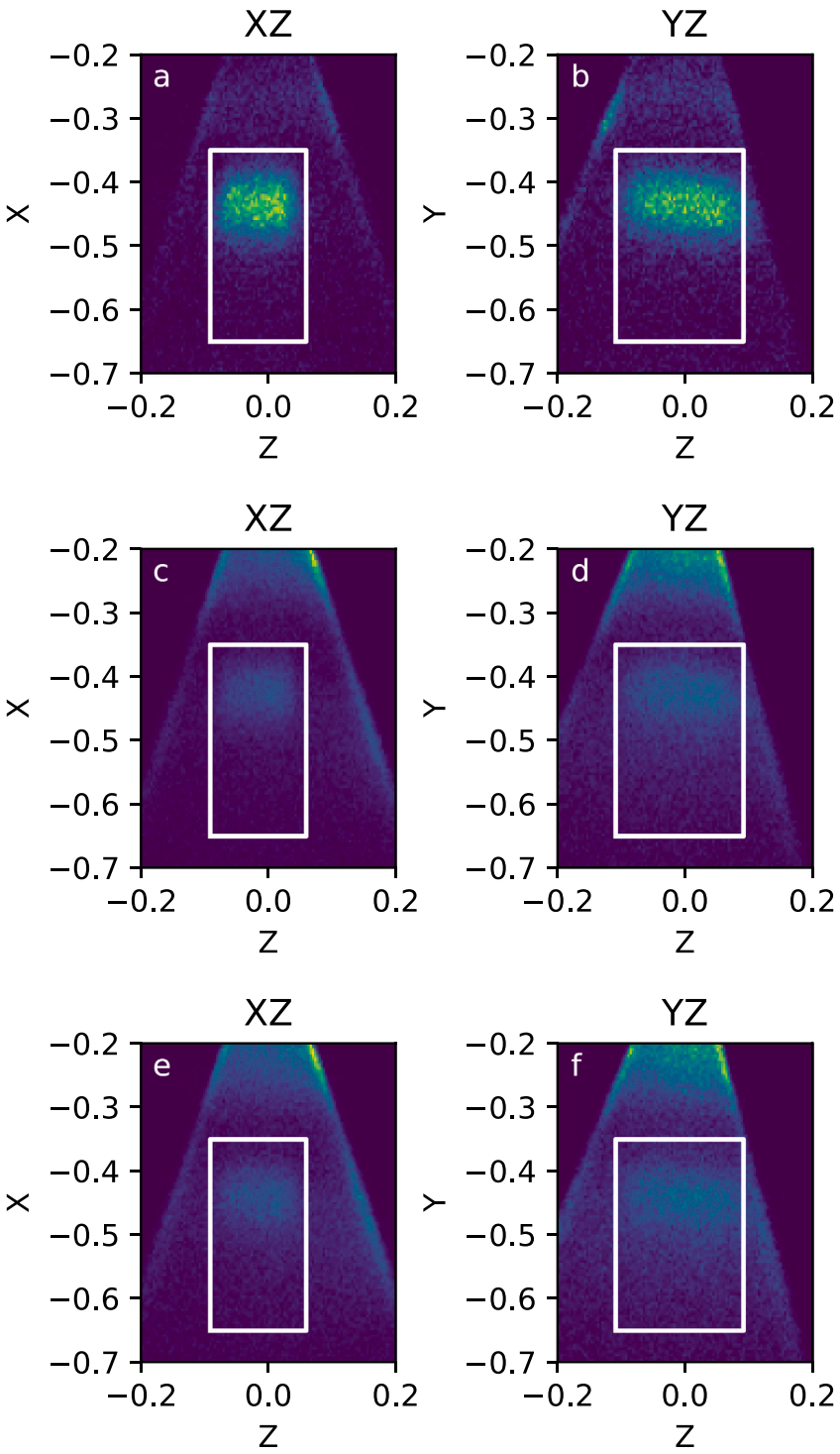


Fig. 3. Voxelized XZ and YZ cross-sections of the reconstructed carbon block signal. (a,b) Steel box only; (c,d) 10 cm soil at 40% VWC; (e,f) 18 cm dry soil. Voxel boundaries capture the carbon block signal without crossing the API cone edge.

Table 2
Results from regressing bulk density (ρ_{bd}) and water content (θ) for 33 modeled soils (Franz et al., 2013) against their regression constants for the double exponential decay in Eq. (5). ρ_{bd} and θ serve as two independent variables in the regression to predict decay constants a, b, and c, according to Eq. (6). Additionally results for the effective values (ρ^*_{bd} and θ^*, as in Eq. (7) and (8)) are shown.

Reaction rate attenuation constants	Regression constants					
	Simple ρ_{bd} and θ			Effective ρ^*_{bd} and θ^*		
	d	e	f	d	e	f
a	−0.103	−0.469	0.081	−0.107	−0.446	0.101
b (cm)	−0.038	3.248	2.631	−0.022	3.067	2.479
c (cm)	−6.835	−15.343	27.559	−6.976	−14.813	28.063

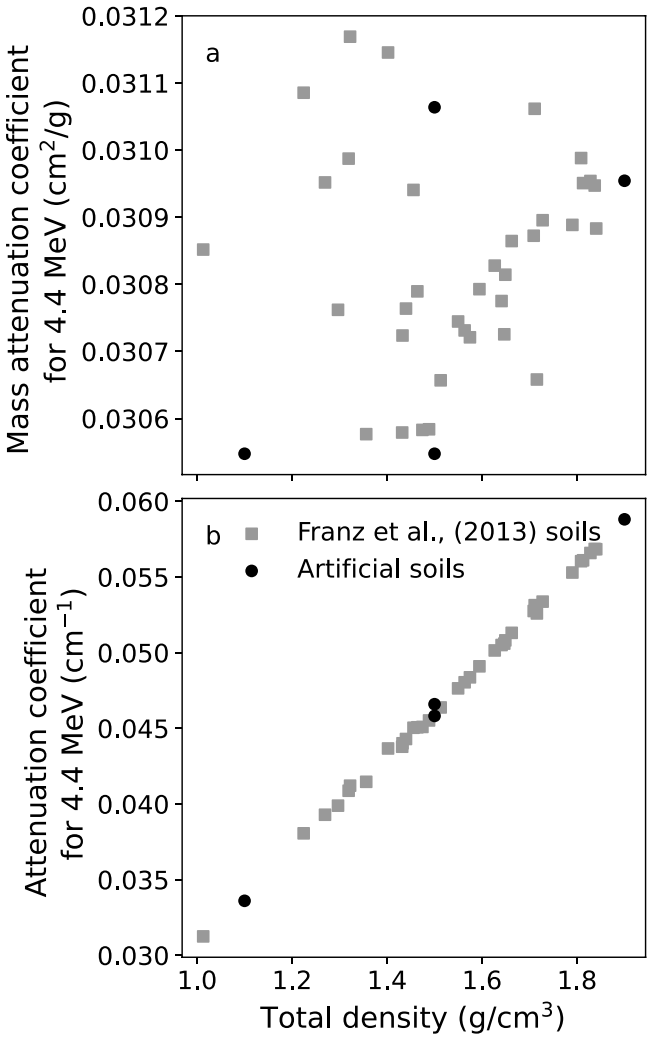


Fig. 4. Mass attenuation coefficients for a 4.43 MeV gamma ray plotted vs. total density of solids and liquids in soil (a). Multiplication by total density yields the linear attenuation coefficient (b).

3.3. Experimental results

In the fixed-depth experiment (10 cm), normalized neutron flux into the carbon block decreased with increasing VWC (Fig. 8). Model predictions matched measured attenuation trends inferred from 4.43 MeV gamma ray counts measured using both NaI and $LaBr_3$ detectors. While the signals from different detectors vary more than expected from just counting statistics (see error bars in Fig. 8), broad model-detector agreement supports the model's ability to predict neutron attenuation from simple field-measurable parameters. In the dry-soil depth experiment (θ = 2.6%), neutron flux decreased with depth in agreement with model predictions (Fig. 9). Agreement was within ~10% at 18 cm depth, consistent with the simulation-based error estimates.

4. Discussion

4.1. Roles of water and solid material in neutron attenuation

Our simulations and experiments show that volumetric water content (θ) is the dominant factor controlling neutron attenuation in soils. This is consistent with the high scattering cross section of hydrogen (Wielopolski et al., 2005), which efficiently moderates fast neutrons. Even modest increases in θ substantially reduce the population of fast neutrons capable of inducing the $^{12}C(n,n'\gamma)$ reaction at 4.43 MeV.

The synthetic soil simulations demonstrate that an increase in water content has a far greater attenuating effect than a mass-equivalent increase in solid material density (Fig. 5). This is because neutron moderation is driven primarily by elastic scattering with light nuclei, and hydrogen is the lightest and most efficient moderator. Dry bulk density (ρ_{bd}) also influences neutron attenuation by increasing the number of nuclei per unit volume, thereby increasing the probability of neutron interactions. However, without hydrogen's moderating effect, the impact is smaller than that of water content per unit mass. Our observation that hydrogenous soil materials more strongly impact neutron attenuation aligns with earlier neutron transport studies in soils (Wielopolski et al., 2008).

4.2. Multiple neutron scattering events

Beyond the magnitude of INS reaction rates, the ratio of 4.43 MeV gammas generated from the interaction of uncollided vs. previously collided neutrons with C varies with moisture content (Fig. 6). The moisture dependence of INS reactions from multiply-scattered neutrons has implications for INS–API: while the alpha detector gives the initial neutron trajectory, multiple scattering events can alter that trajectory before gamma production, introducing spatial uncertainty in voxel reconstructions. Quantifying the magnitude of offset in multiply-scattered neutron trajectories for API events and the resultant error in voxel assignment or spatial resolution warrants further study using detailed particle tracking (e.g., using MCNP's `ptrac` feature).

4.3. Gamma-ray attenuation vs. neutron attenuation

Gamma-ray attenuation at 4.43 MeV depends primarily on total density and is relatively insensitive to soil composition within the range studied (Akar Tarim et al., 2013). Gamma ray attenuation therefore contrasts with neutron attenuation, which is highly sensitive to hydrogen content. As a result, gamma attenuation corrections can be applied using tabulated mass attenuation coefficients and total density measurements, whereas neutron attenuation requires site-specific modeling or empirical correction. Though we excluded gamma attenuation from our experimental setup, it is a necessary factor to consider in a field setting.

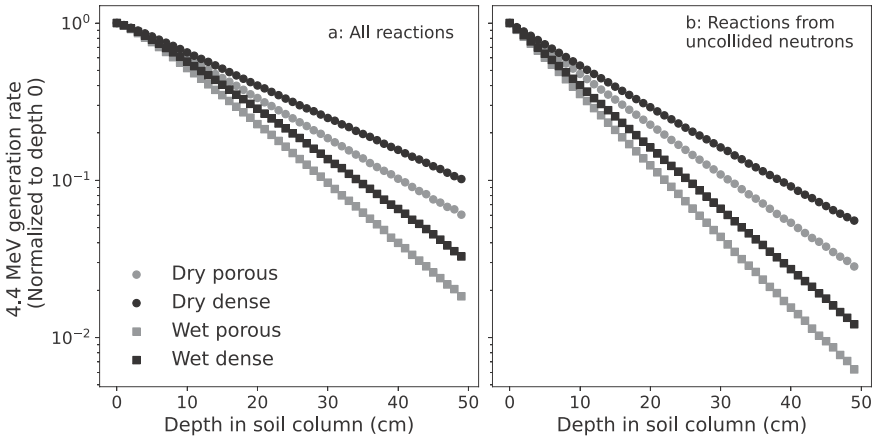


Fig. 5. Normalized 4.43 MeV gamma production vs. depth for four synthetic soils (a) and for uncollided 14.1 MeV neutrons only (b).

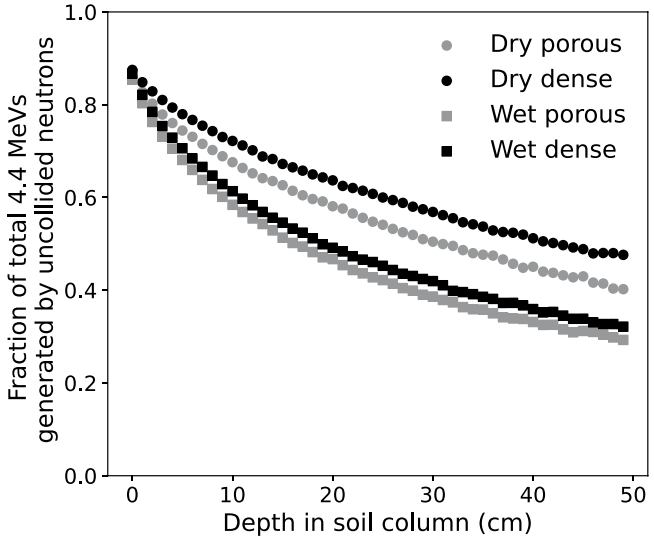


Fig. 6. Fraction of 4.43 MeV gamma rays from uncollided (14.0 MeV to 14.1 MeV) neutrons vs. depth for four synthetic soils.

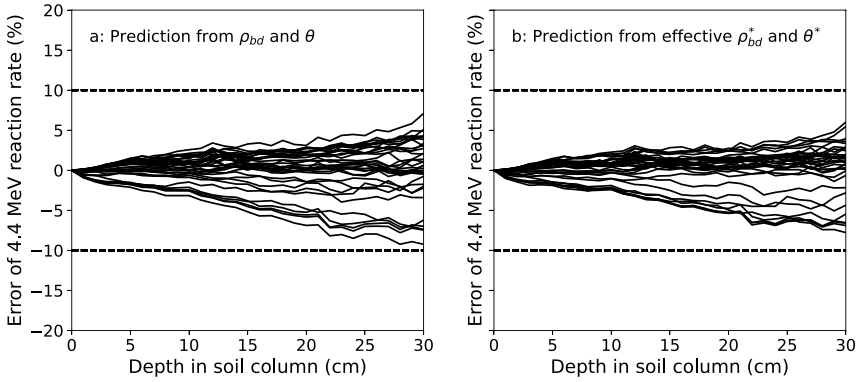


Fig. 7. Percent error between predicted and simulated 4.43 MeV gamma attenuation for 33 soils: (a) using ρ_{bd} and θ; (b) using effective ρ^*_{bd} and θ^*.

4.4. Model practicality and limitations

The regression model developed here requires only ρ_{bd} and θ — quantities that can be measured in the field using standard soil sampling or in situ sensors (Evett et al., 2008). Including lattice and organic water in effective ρ^*_{bd} and θ^* slightly improves performance, particularly in clay-rich or organic-rich soils (Wielopolski et al., 2005). Though the correction framework presented here uses values of bulk density and water content measured by traditional techniques (Franz et al., 2013), both of these inputs can be modeled directly from the measured data itself, which could enable a self-consistent framework that allows for completely non-destructive sampling (Kavetskiy et al., 2026). An additional neutron detector, or running the neutron generator in pulsed mode for a short time, can allow the direct measurement of H concentration in the soil, leading to better moisture estimates (Yakubova et al., 2025; Kavetskiy et al., 2026). Together with the

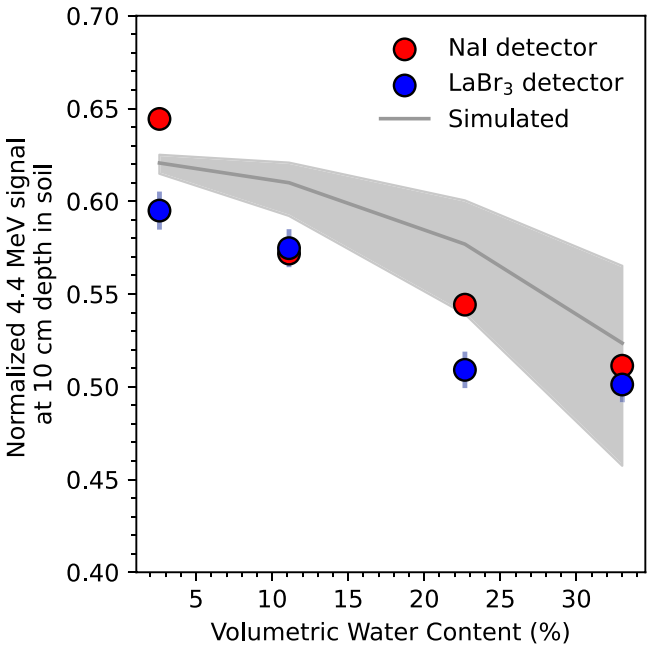


Fig. 8. Gray lines: model predictions for neutron attenuation at 10 cm depth for different VWC. Gray field: range of results using minimum and maximum measured bulk densities as described in Section 2.6. Circles: experimental results from NaI (red) and $LaBr_3$ (blue) detectors. Error bars are around 1% and include counting statistics only.

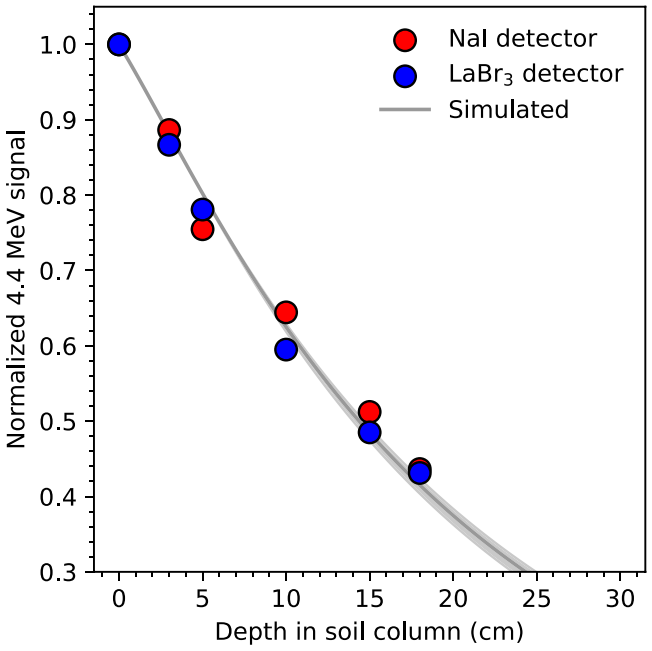


Fig. 9. Gray line: model prediction for dry soil (2.6% VWC). Gray field: range of results using minimum and maximum measured bulk densities as described in Section 2.6. Circles: experimental results from NaI (red) and $LaBr_3$ (blue) detectors. Error bars are around 1% and include counting statistics only.

model presented here, the INS-API data can then be used to provide accurate C estimates without relying on additional measurements.

Importantly, the framework put forth in this study employs a potentially limiting assumption that soil properties are consistent with depth. Signal attenuation may deviate from predictions in layered soils or those with significant contrasts in moisture, texture or organic matter. Our validation experiments were conducted under controlled laboratory conditions using a single soil type; a larger field validation is needed for diverse soils and environmental conditions.

5. Conclusions

We have developed and validated an empirical model that predicts neutron attenuation in soils using only dry bulk density and volumetric water content, addressing a critical source of uncertainty in non-destructive soil carbon measurement by inelastic neutron scattering (INS) techniques. By simulating neutron transport across 33 real and 4 synthetic soil types and verifying results with controlled experiments, we demonstrated that soil water content is the dominant driver of signal attenuation, significantly outweighing the effects of bulk density variations. This finding underscores why simple density-based corrections (standard for gamma methods) are insufficient for neutron-based carbon quantification in soil. The empirical model developed here allows for simple correction of INS-API signals to account for attenuated neutrons at depth.

The regression model presented here describes attenuation profiles with a double-exponential function, achieving predictive accuracy within ~10% at 30 cm depth in simulated soils, validated experimentally up to 18 cm depth. Importantly, this model relies on inputs (ρ_{bd} and θ) that can be derived directly from the multi-elemental spectra provided by the neutron-based measurement system itself. Consequently, this correction framework contributes to a broader suite of literature that aims to enable a fully self-consistent measurement system that can quantify soil carbon stocks without reliance on external, labor-intensive bulk density sampling.

Future work will focus on validating the complete system including bulk density and water estimation from measured data. For researchers and practitioners in precision agriculture, this advancement removes a major barrier to the adoption of INS technology. The correction of signal attenuation at depth ensures that voxelated carbon maps remain quantitatively accurate across changing seasons and moisture regimes, providing the robust, scalable verification needed to assess soil carbon sequestration practices effectively.

CRediT authorship contribution statement

William Larsen: Writing – review & editing, Writing – original draft, Visualization, Validation, Software, Methodology, Investigation, Formal analysis, Conceptualization. **Valerie Smykalov:** Writing – review & editing, Writing – original draft, Visualization, Validation, Software, Methodology, Investigation, Formal analysis, Conceptualization. **Cristina Castanha:** Resources, Methodology. **Eoin Brodie:** Supervision, Funding acquisition, Conceptualization. **Mauricio Ayllon Unzueta:** Validation, Software, Methodology, Formal analysis, Conceptualization. **Bernhard Ludewigt:** Supervision, Methodology, Investigation, Conceptualization. **Arun Persaud:** Writing – review & editing, Writing – original draft, Visualization, Validation, Supervision, Software, Resources, Project administration, Methodology, Investigation, Funding acquisition, Formal analysis, Conceptualization.

Declaration of generative AI and AI-assisted technologies in the manuscript preparation process

During the preparation of this work the author(s) used OpenAI:ChatGPT5 in order to improve the readability of the article. After using this tool/service, the authors reviewed and edited the content as needed and take full responsibility for the content of the published article.

Funding

The information, data, or work presented herein was funded by the Advanced Research Projects Agency-Energy (ARPA-E), U.S. Department of Energy, and the U.S. Department of Energy (DOE) through Lawrence Berkeley National Laboratory's Laboratory-Directed Research and Development (LDRD) as part of its Carbon Negative Initiative, under Contract No. DEAC02-05CH11231. This work was supported in part by the U.S. Department of Energy, Office of Science, Office of Workforce Development for Teachers and Scientists (WDTS) under the Science Undergraduate Laboratory Internship (SULI) program.

Declaration of competing interest

The authors declare the following financial interests/personal relationships which may be considered as potential competing interests: William Larsen reports a relationship with Terradot that includes: employment. If there are other authors, they declare that they have no known competing financial interests or personal relationships that could have appeared to influence the work reported in this paper.

Acknowledgments

We thank Takeshi Katayanagi for mechanical support.

Data availability

Raw data, analysis scripts including some additional plots, and MCNP input files are available at Zenodo (Larsen et al., 2026).

References

Akar Tarim, U., Gurler, O., Ozmutlu, E.N., Yalcin, S., 2013. Monte Carlo calculations for gamma-ray mass attenuation coefficients of some soil samples. Ann. Nucl. Energy 58, http://dx.doi.org/10.1016/j.anucene.2013.03.021.

Alger, R., Raymer, Jr., L., 1963. Formation density log applications in liquid-filled holes. J. Pet. Technol. 15 (03), http://dx.doi.org/10.2118/435-PA.

Ayllon Unzueta, M., Brodie, E., Brown, C., Castanha, C., Gary, C., Pries, C.H., Larsen, W., Ludewigt, B., Rosenstrom, A., Persaud, A., 2019. An associated particle imaging system for soil-carbon measurements. In: Hard X-Ray, Gamma-Ray, and Neutron Detector Physics XXI, vol. 11114, p. 111141B. http://dx.doi.org/10.1117/12.2530704.

Ayllon Unzueta, M., Ludewigt, B., Mak, B., Tak, T., Persaud, A., 2021. An all-digital associated particle imaging system for the 3D determination of isotopic distributions. Rev. Sci. Instrum. 92 (6), http://dx.doi.org/10.1063/5.0030499.

Berger, M.J., Hubbell, J.H., Seltzer, S.M., Chang, J., Coursey, J.S., Sukumar, R., Zucker, D.S., Olsen, K., 2010. XCOM: photon cross sections database. http://dx.doi.org/10.18434/T48G6X, URL https://www.nist.gov/pml/xcom-photon-cross-sections-database.

Borsaru, M., Charbucinski, J., Eisler, P.L., Youl, S.F., 1985. Determination of ash content in coal by borehole logging in dry boreholes using gamma-gamma methods. Geoexploration 23 (4), http://dx.doi.org/10.1016/0016-7142(85)90077-8.

Brown, D.A., Chadwick, M.B., Capote, R., Kahler, A.C., Trkov, A., Herman, M.W., Sonzogni, A.A., Danon, Y., Carlson, A.D., Dunn, M., Smith, D.L., Hale, G.M., Arbanas, G., Arcilla, R., Bates, C.R., Beck, B., Becker, B., Brown, F., Casperson, R.J., Conlin, J., Cullen, D.E., Descalle, M.A., Firestone, R., Gaines, T., Guber, K.H., Hawari, A.I., Holmes, J., Johnson, T.D., Kawano, T., Kiedrowski, B.C., Koning, A.J., Kopecky, S., Leal, L., Lestone, J.P., Lubitz, C., Márquez Damián, J.I., Mattoon, C.M., McCutchan, E.A., Mughabghab, S., Navratil, P., Neudecker, D., Nobre, G.P.A., Noguere, G., Paris, M., Pigni, M.T., Plompen, A.J., Pritychenko, B., Pronyaev, V.G., Roubtsov, D., Rochman, D., Romano, P., Schillebeeckx, P., Simakov, S., Sin, M., Sirakov, I., Sleaford, B., Sobes, V., Soukhovitskii, E.S., Stetcu, I., Talou, P., Thompson, I., van der Marck, S., Welser-Sherrill, L., Wiarda, D., White, M., Wormald, J.L., Wright, R.Q., Zerkle, M., Žerovnik, G., Zhu, Y., 2018. ENDF/B-VIII.0: the 8th major release of the nuclear reaction data library with CIELO-project cross sections, new standards and thermal scattering data. Nucl. Data Sheets 148, http://dx.doi.org/10.1016/j.nds.2018.02.001.

de Gruijter, J.J., McBratney, A.B., Minasny, B., Wheeler, I., Malone, B.P., Stockmann, U., 2018. Farm-scale soil carbon auditing. In: McBratney, A.B., Minasny, B., Stockmann, U. (Eds.), Pedometrics. pp. 693–720. http://dx.doi.org/10.1007/978-3-319-63439-5_23.

Doron, O., 2007. Simulation of an INS soil analysis system.

Evett, S.R., Heng, L.K., Moutonnet, P., Nguyen, M.L., 2008. Field estimation of soil water content: A practical guide to methods, instrumentation and sensor technology. URL https://www.ars.usda.gov/research/publications/publication/?seqNo115=208347.

Franz, T.E., Zreda, M., Rosolem, R., Ferre, T.P.A., 2013. A universal calibration function for determination of soil moisture with cosmic-ray neutrons. Hydrol. Earth Syst. Sci. 17 (2), http://dx.doi.org/10.5194/hess-17-453-2013.

Goorley, T., James, M., Booth, T., Brown, F., Bull, J., Cox, L.J., Durkee, J., Elson, J., Fensin, M., Forster, R.A., Hendricks, J., Hughes, H.G., Johns, R., Kiedrowski, B., Martz, R., Mashnik, S., McKinney, G., Pelowitz, D., Prael, R., Sweezy, J., Waters, L., Wilcox, T., Zukaitis, T., 2012. Initial MCNP6 release overview. Nucl. Technol. 180 (3), http://dx.doi.org/10.13182/NT11-135.

Kavetskiy, A., Yakubova, G., Gautam, S.S., Donner, D.P., Prior, S.A., Allen Torbert, H., 2026. Soil chemical composition and texture determinations using neutron-gamma analysis. Soil Tillage Res. 256, http://dx.doi.org/10.1016/j.still.2025.106912.

Kavetskiy, A., Yakubova, G., Prior, S.A., Torbert, H.A., 2024. Carbon analysis of large soil samples using the tagged neutron method: accounting for radiation attenuation. Appl. Radiat. Isot. 209, http://dx.doi.org/10.1016/j.apradiso.2024.111332.

Lal, R., 2014. Societal value of soil carbon. J. Soil Water Conserv. 69 (6), http://dx.doi.org/10.2489/jswc.69.6.186A.

Larsen, W., Smykalov, V., Castanha, C., Brodie, E., Ayllon Unzueta, M., Ludewigt, B., Persaud, A., 2026. Data, analysis scripts, and simulations files for "field-scale soil carbon analysis: Correcting for moisture and bulk density effects in inelastic neutron scattering". http://dx.doi.org/10.5281/zenodo.18133672.

Padarian, J., Minasny, B., McBratney, A., Smith, P., 2022. Soil carbon sequestration potential in global croplands. PeerJ 10, http://dx.doi.org/10.7717/peerj.13740.

Paustian, K., Collier, S., Baldock, J., Burgess, R., Creque, J., DeLonge, M., Dungait, J., Ellert, B., Frank, S., Goddard, T., Govaerts, B., Grundy, M., Henning, M., Izaurralde, R.C., Madaras, M., McConkey, B., Porzig, E., Rice, C., Searle, R., Seavy, N., Skalsky, R., Mulhern, W., Jahn, M., 2019. Quantifying carbon for agricultural soil management: From the current status toward a global soil information system. Carbon Manag. 10 (6), http://dx.doi.org/10.1080/17583004.2019.1633231.

Sorenson, P.T., Quideau, S.A., Rivard, B., 2018. High resolution measurement of soil organic carbon and total nitrogen with laboratory imaging spectroscopy. Geoderma 315, http://dx.doi.org/10.1016/j.geoderma.2017.11.032.

Spielberg, D., Duneer, A., 1958. Dose attenuation by soils and concrete for broad, parallel-beam neutron sources.

Stanley, P., Spertus, J., Chiartas, J., Stark, P.B., Bowles, T., 2023. Valid inferences about soil carbon in heterogeneous landscapes. Geoderma 430, http://dx.doi.org/10.1016/j.geoderma.2022.116323.

Viscarra Rossel, R.A., Brus, D.J., Lobsey, C., Shi, Z., McLachlan, G., 2016. Baseline estimates of soil organic carbon by proximal sensing: comparing design-based, model-assisted and model-based inference. Geoderma 265, http://dx.doi.org/10.1016/j.geoderma.2015.11.016.

Wielopolski, L., Chatterjee, A., Mitra, S., Lal, R., 2011. *In situ* determination of soil carbon pool by inelastic neutron scattering: Comparison with dry combustion. Geoderma 160 (3), http://dx.doi.org/10.1016/j.geoderma.2010.10.009.

Wielopolski, L., Doron, O., 2012. Nuclear spectroscopy for *in situ* soil elemental analysis: Monte Carlo simulations. Appl. Radiat. Isot. 70, http://dx.doi.org/10.1016/j.apradiso.2011.11.027.

Wielopolski, L., Hendrey, G., Johnsen, K.H., Mitra, S., Prior, S.A., Rogers, H.H., Torbert, H.A., 2008. Nondestructive system for analyzing carbon in the soil. Soil Sci. Am. J. 72 (5), http://dx.doi.org/10.2136/sssaj2007.0177.

Wielopolski, L., Orion, I., Hendrey, G., Roger, H., 2000. Soil carbon measurements using inelastic neutron scattering. IEEE Trans. Nucl. Sci. 47 (3), http://dx.doi.org/10.1109/23.856717.

Wielopolski, L., Song, Z., Orion, I., Hanson, A.L., Hendrey, G., 2005. Basic considerations for Monte Carlo calculations in soil. Appl. Radiat. Isot. 62 (1), http://dx.doi.org/10.1016/j.apradiso.2004.06.003.

Yakubova, G., Kavetskiy, A., Prior, S.A., Torbert, H.A., 2016. Benchmarking the inelastic neutron scattering soil carbon method. Vadose Zone J. 15 (2), http://dx.doi.org/10.2136/vzj2015.04.0056.

Yakubova, G., Kavetskiy, A., Prior, S.A., Torbert, H.A., 2025. Measuring and mapping moisture content in agricultural fields by neutron-gamma analysis. Soil Tillage Res. 248, http://dx.doi.org/10.1016/j.still.2024.106444.

Yakubova, G., Kavetskiy, A., Sargsyan, N., Prior, S.A., Torbert, H.A., 2022. Neutron-gamma analysis of soil for digital agriculture. In: Shamshiri, R.R., Shafian, S. (Eds.), Digital Agriculture, Methods and Applications. IntechOpen, London, http://dx.doi.org/10.5772/intechopen.102128.